Insights into the Adhesive Mechanisms of Tree Frogs using Artificial Mimics

*Dirk-Michael Drotlef, Lukas Stepien, Michael Kappl, W. Jon P. Barnes, Hans-Jürgen Butt, and Aránzazu del Campo**

Elastic, microstructured surfaces (hydrophobic and hydrophilic) mimicking the surface structure of tree-frog toe-pads are fabricated. Their adhesion and friction behaviour in the presence of a liquid layer is evaluated and compared to flat controls. Tree-frog-like patterns are beneficial for wet adhesion only if the liquid does not wet the surface. The situation is different in friction, where the surface structure lead to significantly higher friction forces only if the liquid does wet the surface. Taking into account that tree-frog attachment pads are hydrophilic and that their secretion wets all kind of surfaces, our results indicate that the surface structure in tree-frog toe-pads has been developed for climbing, when shear (friction) forces are involved. These results evidence the benefits and limitations of the surface design (microstructure and hydrophilicity) for adhesion and friction under wet conditions.

1. Introduction

Natural reversible adhesives based on complex topographical designs have attracted scientific interest in the last 10 years. The major attention has been paid to the surface structure of gecko's attachment pads as reversible dry adhesive composed by a dense array of hairs (14 400 setae mm^{-2}) with a particular design of the contact point (*spatulae*).[1] The principle of enhanced adhesion by contact splitting,[2] and the mechanisms that the gecko exploits for directional adhesion and easy release (tilted hairs design)[3] are now well established. Successful gecko-inspired adhesive surfaces[4] and releasing principles[5–6] have been reported. The potential technological applications of these developments are further pushing academic and industrial developments in this area.

Nature also offers interesting examples of reversible attachment under wet conditions. Tree and torrent frogs are able to climb in wet environments without falling. Their toe-pad surface design includes channels and protrusions at different length scales and a fluid secretion.[7–13] In particular, tree-frog toe-pads show a regular hexagonal topography with 10–15 μm epithelial cells separated by ca. 1 μm wide channels. The top of the epithelial cells is subdivided into an array of nanopillars of approximately 300–400 nm diameter, which are terminated in a concave shape.[11] 1–3 μm wide pores are distributed randomly within the array and secrete a watery fluid with unknown properties and unclear role in the attachment process.

Tree-frog adhesive mechanisms are not fully understood, with many of the proposed roles of the different structural features still requiring experimental verification. Reported measurements with living frogs[8–10,12] and a few theoretical studies[7,14,15] have suggested contributions from capillary forces,[15,16] friction forces,[9,14] and viscous forces[10,12] to the wet adhesion mechanism. Theoretical works describe a possible draining effect associated with the channel structures that allows the frogs to expel the fluid out of the contact layer and achieve high frictional forces,[14] as well as highlighting the importance of the contact shape in wet adhesion.[17,18] Possible detachment mechanisms based on a dynamic actuation of the surface topography or liquid amount to switch between adhesive and non-adhesive states have also been theoretically predicted.[19] A possible contribution of the chemical components of the frogs' secretion for attachment or detachment cannot be ruled out.

Experimental evidence on the role of the surface's design for wet adhesion in artificial systems is scarce. Arrays of hydrophobic polymeric micropillars showed a 25% adhesion enhancement in the presence of a thin oil film.[20] The authors explained their results on a combination of surface tension and viscous forces contributing to the adhesion force.[20] Elastomeric microstructured surfaces with T-terminated pillars (diameter 50 μm) showed a 20% increase in adhesion in the presence of a water layer, and a ten-fold higher adhesion than the flat control (also under water).[21] The authors proposed suction forces to be the main contributors, although no experimental verification was provided. Microstructured surfaces containing hexagonal micropillars with narrow channels showed significantly higher friction forces than flat surfaces in the presence of a fluid water layer.[22] The authors claim draining issues and the establishment of direct contact to be responsible for the adhesion enhancement. It is evident that a profound and systematic analysis of the surface design, fluid, and measuring factors is required in order to fully understand wet adhesion

D.-M. Drotlef, L. Stepien, Dr. M. Kappl, Prof. H.-J. Butt, Dr. A. del Campo
Max-Planck-Institut für Polymerforschung
Ackermannweg 10, 55128-Mainz, Germany
E-mail: delcampo@mpip-mainz.mpg.de
Dr. W. J. P. Barnes
Centre for Cell Engineering, University of Glasgow
Glasgow G12 8QQ, UK

DOI: 10.1002/adfm.201202024

mechanisms and to apply them to a rational design of artificial mimics. This manuscript makes a step forward in this direction by comparing the adhesion and friction performance of artificial tree-frog toe-pad mimics with different surface designs and under different and well-defined experimental conditions (wetting/non-wetting liquid, liquid volume, viscosity, and detachment rate). The obtained results provide information about the working principles and mechanisms of adhesion under wet conditions. Obviously non-slipping tires, shoe soles, or reversible medical plasters would greatly benefit from new concepts for adhesion enhancement in wet environments.

2. Experimental Section

Silicon wafers (100 orientation) for photolithography were provided by Crystec (Berlin, Germany).

2.1. Materials and Equipment

SU-8 photoresist types 2005 and 2010 covering a thickness range from 5 to 20 μm and the developer mr-Dev 600 were provided by Micro Resist Technology (Berlin, Germany). Hexadecafluoro-1,1,2,2,-tetrahydro-octyltrichlorosilane used as release agent was purchased from ABCR (Karlsruhe, Germany). Masks for lithography were provided by ML&C (Jena, Germany) in quartz with 0.7×0.7 cm^2 chrome patterned fields. Polydimethylsiloxane (PDMS) prepolymer Sylgard 184 was purchased from Dow Corning (MI, USA). The dental impression elastomer Flexitime Correct Flow was supplied by Heraeus Kulzer Dental (Hanau, Germany).

A mask aligner MJB 3 UV 400 (Süss MicroTec Lithography, Garching, Germany) was used for lithography. A PL-360 LP filter (Omega optical, Brattleboro, USA) was used for cutting wavelengths shorter than 350 nm during the exposure step. A spin-coater WS-650SZ-6NPP/LITE/IND (Laurell Technologies Corporation, North Wales, USA) was used for preparation of photoresist films. Baking steps were carried out on a Präzitherm heating stage (LHG, Düsseldorf, Germany). Surface microstructures were characterized by scanning electron microscopy (SEM; LEO 1530VP Gemini, Carl Zeiss Jena, Oberkochen, Germany). The profiles of the microstructures were measured with a confocal microscope μSurf c (NanoFocus AG, Oberhausen, Germany). Plasma treatment of samples was carried out with a Plasma Activate Statuo 10 USB chamber (Plasma Technology GmbH, Rottenburg, Germany). The static contact angles were measured by a DSA10-Mk2 instrument (Kruess, Hamburg, Germany).

2.2. Fabrication of SU-8 Micropatterns by Optical Lithography

Wafers were cleaned in piranha solution (5:1 H_2SO_4/H_2O_2) overnight and rinsed with deionized water. The wafers were transferred into the cleanroom, rinsed with acetone and blown dry with nitrogen before SU-8 lithographic processing. Masks containing several 0.7×0.7 cm^2 patterned fields with either a chrome hexagonal network (period 10 to 20 μm, width 1–5 μm) or chrome micrometric hexagons (diameter 10–20 μm, spacing 1–5 μm) were used. The processing parameters for the hexagonal patterns with 5, 10, and 20 μm layer thickness are specified in Table SI-1 in the Supporting Information. The obtained hexagonal patterns were used as moulds for the subsequent replication processes with PDMS.

Before replication, the surface of the SU-8 patterned wafers was modified with a perfluorinated coating to avoid mould sticking. This was performed by gas phase silanization in an evacuated desiccator for 30 min using 20–50 μL of hexadecafluoro-1,1,2,2-tetrahydrooctyltrichlorosilane followed by heating for 30 min at 95 °C in a vacuum oven. Silanization increased the contact angle of the silicon wafer from 10° to 113° and of the cured SU-8 pattern from 73° to 115°.

2.3. Fabrication of PDMS Hexagonal Pillar Patterns by Soft-Moulding

Different reported soft-moulding strategies were used in order to obtain arrays of hexagonal micropillars with different tip geometries made of PDMS. PDMS is a soft elastomeric material with a Young's modulus of approximately 2 MPa, close to the reported 5–15 MPa Young's Modulus of tree-frog toe-pads at the epithelial surface.[11] **Figure 1** shows representative SEM images of pillar arrays and the profile of the pillars and their dimensions as obtained with the confocal microscope.

2.3.1. Patterns of Flat Terminated Pillars by Direct Replication of SU8 Masters

A 10:1 ratio of Sylgard 184 prepolymer and crosslinker was mixed, degassed, poured onto the SU-8 patterned wafer with the hexagonal network and cured for 14 h at 65°C in a vacuum oven. The total thickness of the PDMS layer was 1 mm. Micropatterned PDMS fields with arrays of hexagonal pillars with 19 μm diameter, 5 to 20 μm height and separated by 1 to 3 μm wide channels were obtained. The hexagonal pillars had sharp edges (in contrast to those obtained by double moulding, see below)

2.3.2. Patterns of Flat Terminated Pillars by Double Soft-moulding[23–25]

A 10:1 ratio of Sylgard 184 prepolymer and crosslinker was mixed, degassed, poured onto the SU-8 patterned wafer with hexagonal pillars and cured for 14 h at 65 °C in a vacuum oven. The obtained Sylgard pattern (hexagonal network) was plasma treated for 10 min followed by a silanization by vapour exposure in vacuum to hexadecafluoro-1,1,2,2-tetrahydrooctyltrichlorosilane for 30 min, followed by a curing step at 95 °C for 30 min. The plasma treatment and silanization are essential for avoiding sticking in the next moulding step. A 1:10 ratio of Sylgard 184 prepolymer and crosslinker was cast onto the perfluorinated PDMS pattern and cured at 65 °C for 14 h and then demoulded. Micropatterned PDMS fields with arrays of hexagonal pillars with 7 to 15 μm diameter, 5 to 20 μm height and separated by 4 to 8 μm wide channel were obtained. The total thickness of the sample was 1 mm. Pillars obtained by double moulding had rounded edges.

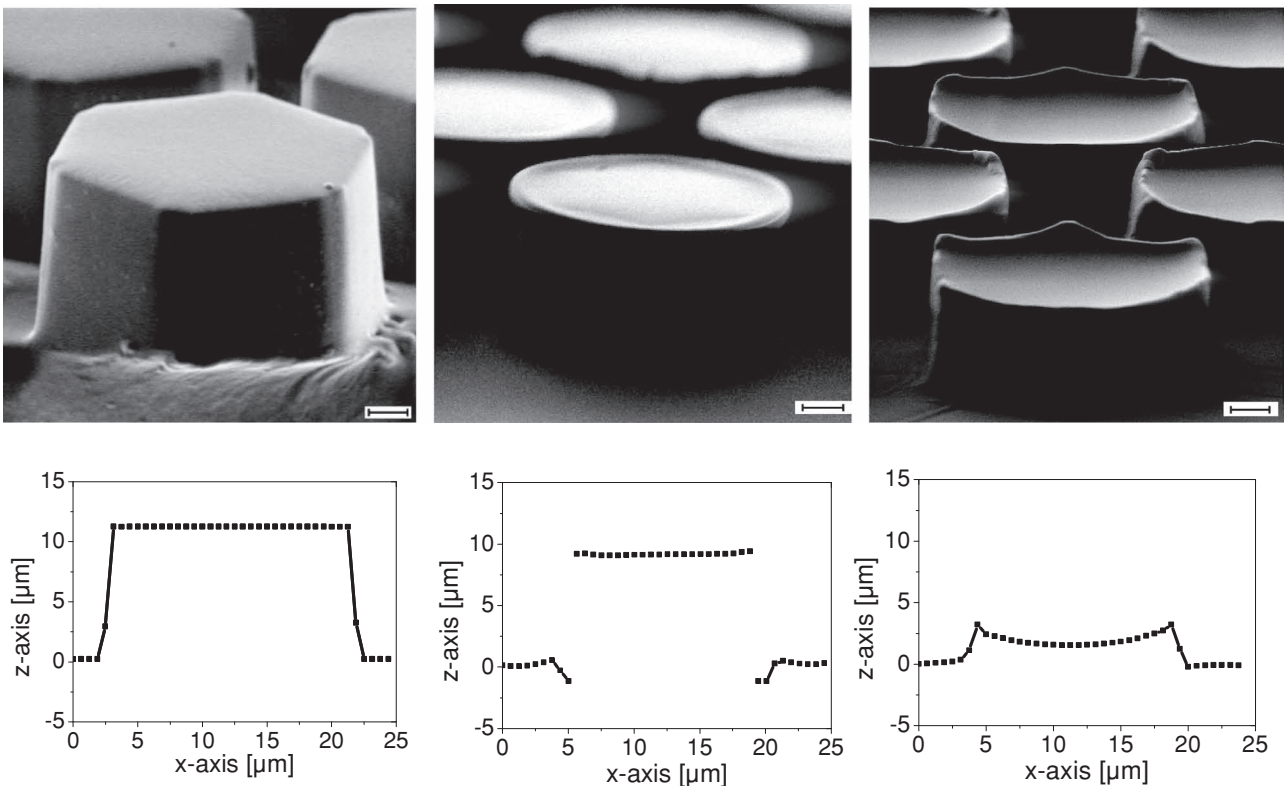

Figure 1. SEM images of PDMS arrays of hexagonal micropillars (15–19 µm diameter) terminated with flat tips, T-shaped tips (10 µm height, 3 and 5 µm channel width) and concave tips (3 µm height, 5 µm channel width). Scale bars correspond to 2 µm. Below, the corresponding profiles of the pillars as obtained with a confocal microscope are shown. Note that this method cannot image the side walls of the pillars, especially if there are overhangs (T-shaped tips).

2.3.3. T-Shape Terminated Pillars Obtained by Inking and Printing[23,26]

Sylgard 184 prepolymer and crosslinker (ratio 10:1) were mixed and degassed. A thin film (0.6 –1 µm) was dragged onto a glass plate using a film applicator (Erichsen, Hemer, Germany) and left for 30 min. A PDMS pattern with flat terminated hexagonal pillars was manually inked into the liquid PDMS film, pressed against a glass slide and cured for 1 h at 90 °C. Micropatterned PDMS fields with arrays of hexagonal pillars with 16 µm diameter, 10 µm height and separated by 5 µm wide channel were obtained.

2.3.4. Fabrication of Hexagonal Pillars with Concave Tips[27]

Sylgard 184 prepolymer and crosslinker (ratio 10:1) were mixed and degassed, poured onto a glass Petri dish and precured for 5–6 min at 90 °C. A PDMS mould was pressed against the precured PDMS film and a 125 g weight was applied. The sample was cured for 55 min at 90 °C. Micropatterned PDMS fields with arrays of hexagonal pillars with 15 µm diameter, 10 µm height, and separated by 5 µm wide channel were obtained.

The surface of the obtained PDMS patterns was modified to make them hydrophilic by treatment in oxygen plasma (80 W, 0.1 mbar O_2, 5–10 s). Under these conditions a hydrophilic silica surface layer (contact angle < 10°) was generated without significant change in the surface roughness and mechanical properties of bulk PDMS. Longer or higher intensity plasma treatment increased the surface roughness and cracks appeared at the surface. Plasma treatment was performed directly before the adhesion measurement and samples were kept in water in order to avoid hydrophobic recovery at the surface and maintain the hydrophilic character over time.

Flat PDMS films were prepared for control measurements. A 10:1 ratio of Sylgard 184 prepolymer and crosslinker was mixed, degassed, poured onto a glass petri dish and cured for 14 h at 65 °C. The side exposed to the Petri dish was used for adhesion measurements. The total thickness of the sample was 1 mm.

2.4. Contact Angle (CA) Measurements

Static contact angles were measured by the sessile drop method, placing a 10 µL water drop onto the sample with a microsyringe. At least five measurements were performed on each sample. Advancing and receding contact angles were measured placing a 10 µL drop onto the sample with a microsyringe and first increasing and then decreasing its volume by 1 µL s^{-1}. The advancing contact angle was measured when the drop reached the maximum volume before increasing the contact area and the receding contact angel was measured when the drop had

the lowest volume before decreasing the contact area. At least five measurements were performed on each sample.

2.5. Adhesion Testing

The adhesion force of flat and structured surfaces was measured using a custom-built equipment consisting of a ruby sphere (4 mm diameter) mounted at the end of a cantilever with a thin film force sensor (Supporting Information, Figure SI-1). The sample was periodically moved up and down at constant speed by a piezo translator while recording the force. The recorded force-versus-piezo position curves were converted to force-versus-distance curves by adding the deflection of the cantilever to the position. In the following we call force-versus-distance briefly "force curves". The adhesion force is the force required to pull the sphere from the sample surface. The approach and retract speed could be adjusted between 5 and 200 μm s^{-1}. The contact time and delay time between single force curves could be set independently. The maximum force that could be recorded was 200 mN. The noise of the detection system was less than 10 μN.

Glycerol was selected as polar fluid since it does not evaporate during the measurements and, therefore, it allows accurate control over the amount of liquid at the fluid joint. 99% Glycerol has a surface tension of 0.064 N m^{-1} and a viscosity of 1146 mPa s at 20 °C (water surface tension is 0.0728 N m^{-1} and viscosity 1.002 mPa s). The fluid was applied to the contact surface by means of a micropipette. The advancing and receding contact angles of glycerol on the ruby sphere were 64° and 41°, respectively.

The value of the radius of the meniscus (l) for the theoretical calculation of the adhesion force was obtained by imaging the contact surface from below with a video microscope. In order to obtain single drops on the top of each pillar (Section 3.2), a drop of glycerol was first applied onto the hydrophobic microstructured surface and the substrate was tilted. The drop rolled over the micropillars and small droplets remained attached to each pillar. These small droplets were transferred to the hydrophilic microstructured surfaces by contact printing.

Since the mechanical properties of PDMS may change over time, all adhesion experiments were performed on one-day-old samples fabricated under the same experimental conditions, unless specified. The laboratory temperature and humidity were recorded for each measurement and were in the range of 20 to 25 °C and 20% to 35% humidity. A minimum of 5 measurements was performed for each data point and measurements were performed with at least three different samples prepared on different days. For control purposes, adhesion tests under the same conditions were also conducted with flat specimens.

2.6. Friction Testing

Friction measurements were performed using a custom-built equipment (see Supporting Information, Figure SI-2).[28] Friction experiments were performed by attaching the patterned substrate of flat control (0.7 × 0.7 mm^2) to a bending beam and measuring against a glass sphere of 1 cm diameter. Before the experiment 0.5 μL of water was applied to the PDMS sample. The samples were brought in contact with the probe, a load of 1 mN was applied and kept constant during the measurement using force feedback. The sample was moved at 100 μm s^{-1} over a distance of 6 mm. During the experiment, the contact area was recorded by a camera attached to a stereo microscope.

3. Results and Discussion

3.1. Adhesion of Flat vs. Microstructured Surfaces

3.1.1. Description of Force Curves

Figure 2 shows typical force curves obtained for flat and microstructured (flat tips) hydrophobic and hydrophilic surfaces in the presence of 0.1 μL glycerol. Before the experiment was run, the glycerol drop was placed at the bottom part of the ruby sphere with a micropipette under microscopic control. The flat or patterned surfaces were brought into contact with the ruby sphere, compressed up to a prefixed displacement (loading cycle), and retracted. Repulsive forces were counted as being positive, and attractive forces as negative.

Hydrophilic Surfaces (Wetting Case): When the glycerol drop on the ruby sphere approached the hydrophilic PDMS surface (flat or structured), a snap-in event was visible in the force curves, followed by a long-range attractive force. This was attributed to attractive capillary forces between the hydrophilic surface and the wetting glycerol. Note that the advancing contact angle of glycerol on hydrophilic PDMS was 10°, and the receding contact angle was < 10°. The jump-in occurred at a shorter distance on the microstructured surface. This suggests that the volume of the glycerol drop on the top of the patterned surface was smaller because part of the fluid filled the channels. In the retraction cycle a long range attractive force was detected and attributed to capillary forces. These features were common for flat and microstructured surfaces.

To demonstrate the occurrence of capillary attraction, the long-range attractive forces in Figure 2 were fitted for a sphere–plane model for capillary forces assuming constant volume.[29] The theoretical capillary force was calculated by:[30]

$$F_C = 4\pi\gamma c R\left(1 - \frac{D}{\sqrt{\frac{V}{\pi R} + D^2}}\right) \quad \text{with } c = \frac{\cos(\theta_1 + \beta) + \cos\theta_2}{2} \tag{1}$$

Here, γ is the surface tension of the liquid, R is the sphere radius, β is the angle describing the position of the liquid meniscus, Θ_1 and Θ_2 are the contact angles of the liquid to the sphere and the plane, and D is the gap width (see Supporting Information, Figure SI-6). V is the volume of the liquid meniscus. Since glycerol does not evaporate, V was assumed to be constant. Using an optical microscope we estimated β = 10° ± 10°. Since this value may change for different approaches and depending on the situation, we used c as a fit parameter.

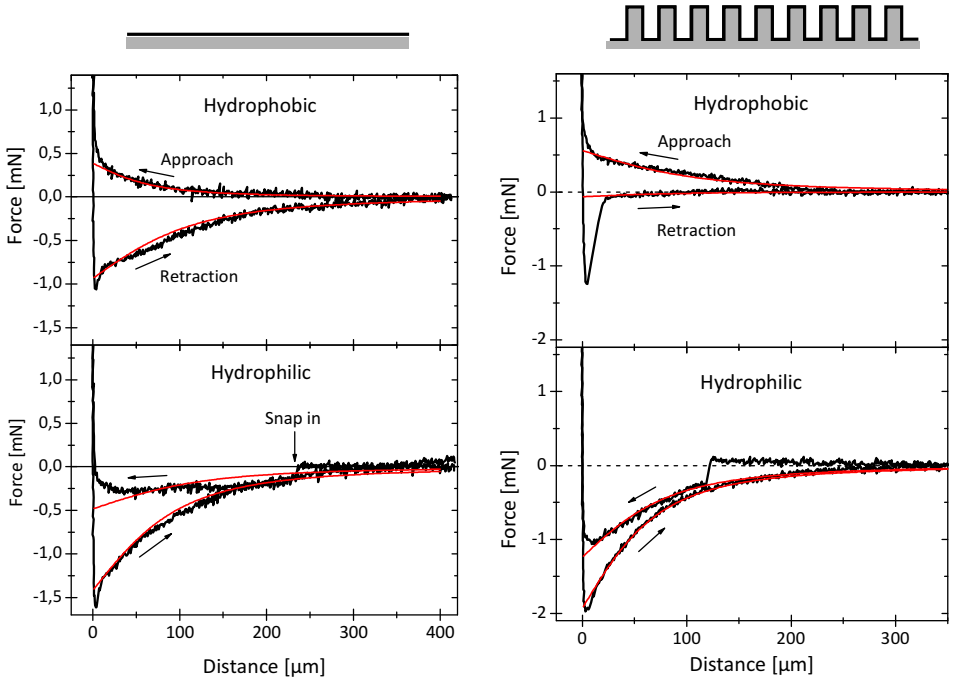

Figure 2. Force–distance curves recorded with flat and microstructured (planar tip geometry) hydrophobic and hydrophilic surfaces in the presence of 0.1 μL glycerol. Microstructured surfaces were obtained by double moulding and had pillar diameter = 15 μm, pillar height = 10 μm, channel width = 5 μm. The red line represents the theoretical capillary force as a function of distance (0–400 μm) calculated with $\gamma = 0.064$ N m^{-1}, $R = 0.002$ m, and $c = -0.24$, $V = 4 \times 10^7$ μm^3 (approach flat hydrophobic); $c = 0.58$, $V = 11 \times 10^7$ μm^3 (retraction flat hydrophobic); $c = 0.3$, $V = 13 \times 10^7$ μm^3 (approach flat hydrophilic); $c = 0.88$, $V = 8 \times 10^7$ μm^3 (retraction flat hydrophilic); $c = -0.35$, $V = 10^8$ μm^3 (approach microstructured hydrophobic); $c = 0.04$, $V = 6 \times 10^7$ μm^3 (retraction microstructured hydrophobic); $c = 0.77$, $V = 5.6 \times 10^7$ μm^3 (approach microstructured hydrophilic); $c = 1.2$, $V = 4.3 \times 10^7$ μm^3 (retraction microstructured hydrophilic).

The red curves in Figure 2 show that the theoretical curves nicely fit the experimental results. For the retracting force curve with $\gamma = 0.064$ N m^{-1}, and $R = 2$ mm the curve could be fitted with $V = 1.2 \times 10^8$ μm^3.

Hydrophobic Surfaces (Non-wetting Case): When the sphere approached the hydrophobic surfaces, flat or microstructured, a long-range repulsion was first detected. This was attributed to capillary forces between the hydrophobic surface and the hydrophilic, non-wetting glycerol (advancing CAs of glycerol on flat and structured surfaces were 110° and 146° respectively (Supporting Information, Table S2)). During retraction from the flat surface, a short-range and a long-range attractive contribution to the force were detected. We attributed the short-range contribution to adhesion by direct contact between the sphere and the PDMS surface. This contribution was dominant in the microstructured surface, possibly because the channel structure allowed draining of glycerol out of the contact surface and multiple direct contacts between the sphere and the top of the pillars could be established. The long-range contribution was attributed to capillary forces. These were attractive on the flat surface because the receding contact angle of the flat surface (89°) was slightly below 90°. However, on the microstructured surface capillary forces were repulsive because the receding contact angle (117°) was above 90°. Note that these features were common to all microstructured surfaces independently of their contact geometry (flat, T-, or concave shape). These results point out a significant difference in the ratio of capillary to direct contact forces in the adhesion force of hydrophobic flat and microstructured surfaces.

In all cases the force curves could be fitted with the capillary force given in Equation 1. The volume of the liquid in the fitting was roughly 10% of the amount applied in the experiment. The values for c obtained followed the trend expected when calculating the value with Equation 1 for $\beta = 10° \pm 10°$ (Supporting Information, Table S2).

3.1.2. Adhesion Forces

The experimental value of the pull-off force, F_{off}, was extracted from the minimum of the retraction curves. In the following, we call this the adhesion force.

Hydrophilic Surfaces (Wetting Case): Adhesion forces measured on hydrophilic flat and microstructured surfaces with planar, T-, or concave tip shapes were indistinguishable (**Figure 3**). The adhesion force was also independent of pillar height, pillar width or interpillar distance (pillar diameter = 19 μm channel width = 1, 2, or 3 μm; channel depth = 5, 10, or 20 μm and pillar diameter = 7, 11, or 15 μm, channel width = 5 μm; channel depth = 5, 10, or 20 μm) (Supporting Information, Figure SI-3 to SI-5). In summary, adhesion onto hydrophilic surfaces was driven by capillary forces caused by a single meniscus spanning over the flat or structured surface, and a contact line that was neither influenced by the presence of the microstructure nor by the microstructure geometry.

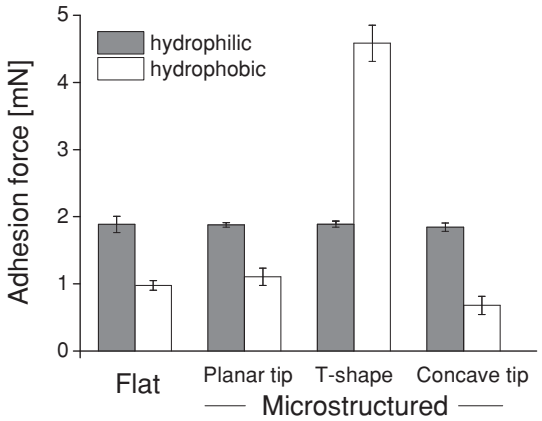

Figure 3. Adhesion force of flat and patterned surfaces in the presence of 0.1 µL glycerol. Microstructured surfaces had different contact geometries: planar, concave, and T-shape. Pillar diameter = 15 µm, pillar height = 10 µm, channel width = 5 µm.

Hydrophobic Surface (Non-wetting Case): The adhesion force of hydrophobic flat surfaces in the presence of 0.1 µL glycerol was different from that on microstructured surfaces. The biggest difference was obtained on T-shape microstructures which showed a five-times higher adhesion force than the flat surface (Figure 3). The hydrophobic microstructured surface with flat terminated pillarsm showed a slightly higher adhesion force than the flat one, while concave terminated micropillars showed a 30% lower adhesion than the flat surface. These differences can be explained on the basis of the force curves described above (Figure 2). These showed two contributions to the adhesion force: a long-range capillary component and a short-range direct contact component. The direct contact component was dominant on microstructured surfaces. Our previously reported work demonstrated that the direct contact force ("dry contact") of structured surfaces is strongly influenced by the contact geometry.[23,26,27] T-shaped microstructured surfaces showed significantly higher dry adhesion performance than planar terminated ones.[23,26,27] Figure SI-7 in the Supporting Information confirms this behaviour in our hydrophobic hexagonal patterns. Consequently, the differences in the adhesion force of the hydrophobic patterns in the presence of non-wetting glycerol respond to their different direct contact forces. This is confirmed by the preload dependence of the adhesive force (Supporting Information, Figure SI-8), which is a unique characteristic of dry patterned adhesives (Supporting Information, Figure SI-7 and and work by Arzt and co-workers[23,24]). Note that only a fraction of the dry adhesion force is achieved by direct contact under wet conditions (Supporting Information, Figure SI-9).

The theoretical contribution of the capillary forces to the adhesion was calculated with Equation 1 taking $\gamma = 0.064$ N m^{-1}, $R = 0.002$ m, $\Theta_1 = 0°$ and $\Theta_2 = 110°$ for glycerol on hydrophobic PDMS, $D = 0$, the experimental value of $l = 350$ µm for our experiment, $V = 0.1$ µL, and the calculated values of β. A value of $F_c \approx 0.5$ mN was obtained. Note that the theoretical value of capillary forces on hydrophobic substrates is notably smaller than on hydrophilic ones (Supporting Information, Figure SI-10). However, this value only represents *ca.* one-half of the measured total adhesion force on flat hydrophobic substrates (1.0 mN). The additional 0.5 mN is attributed to two effects. First, the direct contact between the PDMS and the ruby surface. For an estimation of the contact force we apply JKR theory.[31] According to JKR theory the work of adhesion per unit area w is related to the adhesion force by $F = 3\pi w R/4$. With $F = 0.5$ mN we obtain a contribution of short range forces of $w \approx 0.3$ N m^{-1} for the hydrophobic flat surface. The second effect relates to the assumption that the elastic surface deformation is negligible compared to the radius of the sphere, which was made in the derivation of Equation 1. PDMS is so soft that this assumption is not strictly fulfilled. In fact, we have recently demonstrated that for soft surfaces the capillary force is higher than calculated by Equation 1.[15]

These results demonstrate that hydrophobic hexagonal patterns can be beneficial for adhesion under wet conditions depending on the topographical design. Note that in a previous paper, hydrophobic T-terminated pillars (diameter 50 µm) were reported to show a ten-fold increase in adhesion underwater against the flat controls.[21] These results are also in agreement with our microstructured surfaces measured with a water drop (see Supporting Information, Figure SI-11). However, the authors claimed suction forces to be the main contributors (though no experimental evidence was provided). Our results demonstrate that the combination of capillary and direct contact forces alone explain this behaviour. Suction forces do not seem to play a role.

3.2. Influence of Liquid Volume

Adhesion measurements onto hydrophobic and hydrophilic flat and microstructured surfaces using different glycerol volumes were performed. **Figure 4**a represents force curves for hydrophilic surfaces measured in three different wet scenarios: I) glycerol drops only on top of the micropillars, and, II) 0.1 µL, and III) 0.2–0.4 µL glycerol transferred from the ruby sphere. When the sphere approached the wet surface in state I, a jump in was observed at a typical distance of 5 µm. At this point contact between the ruby sphere and the drops on the micropillars was established. Afterwards multiple menisci were formed and capillary forces attracted the sphere towards the microstructured surface. On retraction only a short-range attractive force was observed.

When increasing the liquid volume (state II) the jump-in occurred at a larger distance (20 µm) and a long-range attractive force was observed in the loading cycle. On retraction an attractive force was observed over a longer distance. Both attractive forces are attributed to capillary forces. A larger liquid volume (state III) extends the range of action of the capillary forces.

The adhesion forces measured on the microstructured surface (Figure 4b) increased from state I (1.1 mN) to state II (1.9 mN). This means that splitting a single capillary into the small capillary bridges (state II vs. I) is not beneficial for adhesion purposes. The adhesion enhancement by contact splitting,[2] which has been proved to be an important design rule for dry adhesives,[24] does not seem to help for our wet case. It is important to note that reported theoretical models have identified other surface designs where the multiple capillary bridges

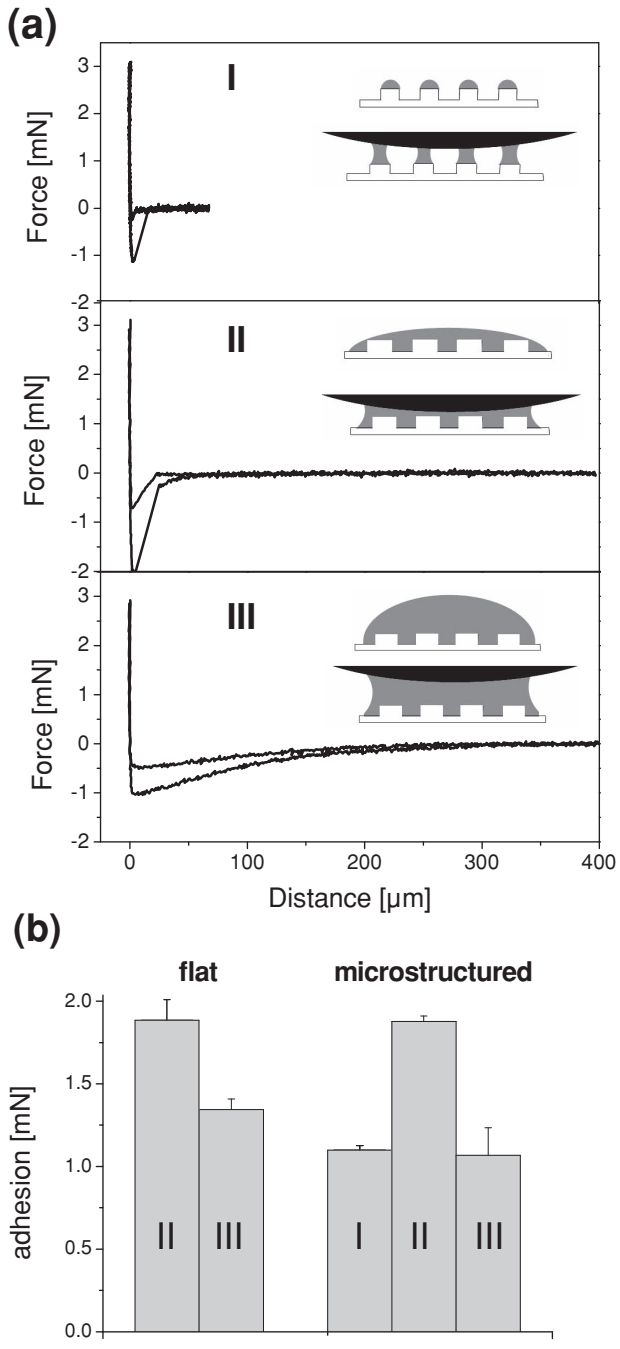

Figure 4. a) Force curves measured on hydrophilic microstructured surfaces in the presence of different volumes of glycerol: only droplets on top of pillars (state I), 0.1 μL (state II) and 0.2–0.4 μL (state III). Pillar diameter = 15 μm, channel width = 5 μm; channel depth = 10 μm obtained by double moulding. b) Adhesion forces for flat and microstructured surfaces with different amounts of glycerol present.

seem to be favourable for adhesion purposes.[32] The decrease in the adhesion force with increasing fluid volume (1.9 mN in state II *vs.* 1.1 mN in state III) also agrees with an adhesion mechanism based on capillary forces. A higher fluid volume causes a decrease in F_c according to Equation 1 (see Supporting Information, Figure SI-12 for a graphic representation). It is important to note that similar results were measured on surfaces with different geometries.

On hydrophobic surfaces, capillary forces only make a small contribution to adhesion force (Figure 2) and, therefore, adhesion force did not significantly change with liquid's volume.

3.3. Adhesion Dependence on Viscosity and Retracting Rate

Adhesion measurements onto hydrophilic flat and structured surfaces were performed varying the approaching/retracting rate of the cantilever (5, 50, and 200 μm s^{-1}) and the viscosity of the liquid (mixtures of water and glycerol with viscosities between approximately 1 and 1000 mPa s). No differences in the adhesion force were detected when measuring with liquids with different viscosity (**Figure 5**). However, an increase in the adhesion force was detected on the flat surfaces when increasing the retracting rate, suggesting a possible hydrodynamic contribution to the adhesive force. However, analogous measurements performed under dry conditions showed similar rate dependence. This indicates that these effects are not related to hydrodynamic forces but to dissipation in the PDMS during pull-off. A rate dependence adhesion to PDMS surfaces has been observed before.[33–36] It was attributed either to viscous dissipation at the rim of the contact zone during crack propagation,[33,34] or to diffusion and entanglement of interfacial polymer chains.[35,36] In summary, hydrodynamic forces do not seem to play a role in wet adhesion under our experimental conditions.

3.4. Friction

Representative friction curves of hydrophilic flat and structured substrates in the presence of 0.5 μL water are shown in

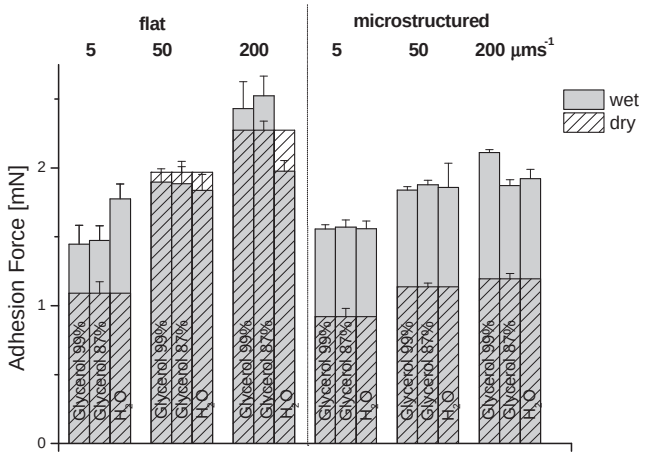

Figure 5. Adhesion force measured on hydrophilic flat and structured (pillar diameter = 15 μm, channel width = 5 μm; channel depth 10 μm, obtained by double moulding) surfaces at different rates (5, 50, and 200 μm s^{-1}). Measurements were performed in dry conditions and in the presence of 0.1 μL fluid (corresponding to state II in Figure 4) with different viscosities (glycerol 99% with viscosity 1146 mPa s; glycerol 87% (mixed with water) with viscosity 120 mPa s; water with viscosity 1.002 mPa s).

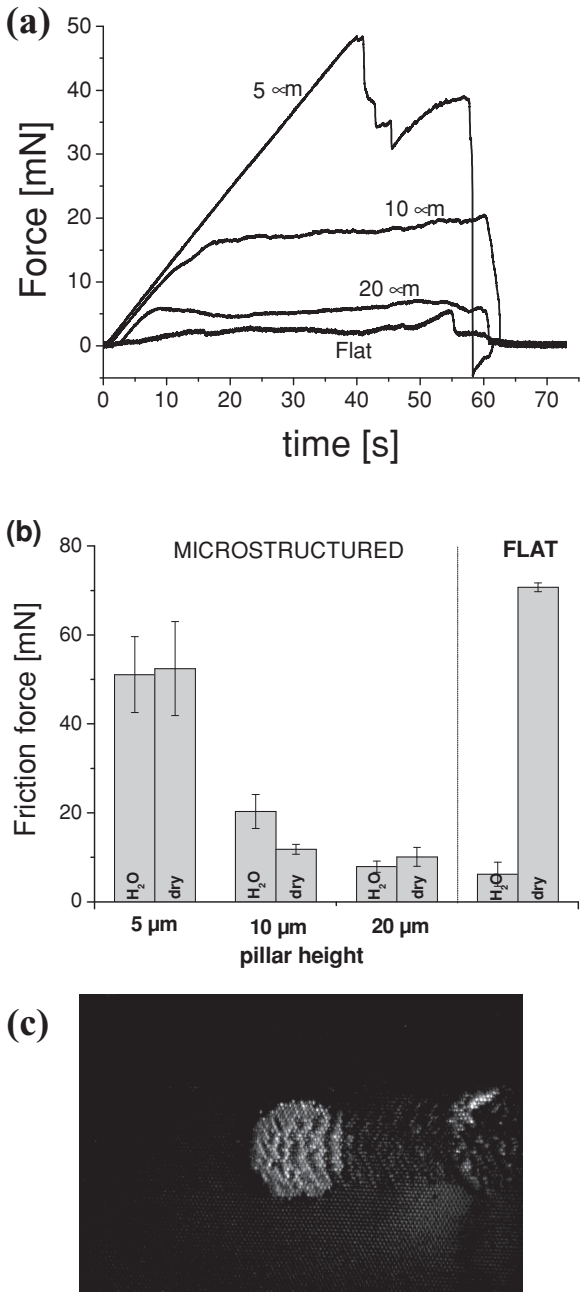

Figure 6. a) Friction curves measured on flat, hydrophilic hexagonal patterns (pillar diameter = 15 µm, channel width = 5 µm; channel depth = 5, 10, and 20 µm) in the presence of 0.5 µL water. b) Friction force of hydrophilic hexagonal patterns and flat controls in the presence of 0.5 µL water and under dry conditions (Supporting Information, Figure SI-13 shows the original friction curves in dry conditions) with a constant velocity of 100 µm s^{-1}. c) Microscopic image of the structured surface (20 µm channel depth) during a friction experiment. The sphere slides from right to left. Bent pillars that stick together can be observed across the sliding path of the sphere and also within the contact area.

Figure 6a. The experiment started by bringing the wet sample into contact with the probe followed by application of a constant shear force. On the flat substrate the sphere easily slid over the surface and a low and constant friction force was detected. The liquid mainly acted as a lubricant. On the micropatterned surface with pillars of 5 µm height the sphere initially stuck (static friction). When the applied shear force reached the limit of the static friction, the probe slid over the sample and a saw-tooth like profile was observed, indicating a stick-slip friction mode. The stick-and-slip events are associated with rows of pillars detaching from the surface while new ones came into contact. On micropatterned surfaces with pillars with higher aspect ratio, a much lower static friction and a constant sliding friction force was detected.

The maximum friction force measured for the different geometries is represented in Figure 6b. A friction force of 52 mN was obtained for the structured surface with 5 µm height hexagonal pillars, whereas negligible friction was detected on the flat surface. This result demonstrates a beneficial role of the surface pattern for increasing frictional forces in attachment when a wetting fluid is present. The increased friction on the structured surface can be attributed to two reasons, as follows. i) The drainage of the liquid through the channels out of the contact surfaces and the establishment of dry contact between the probe and the tip of the pillars. This hypothesis is supported by the fact that the friction value of the structured surface in the presence of water was the same as in dry conditions. Draining the fluid out of the contact surface cannot occur on a flat surface, where the liquid acts as a lubricant. ii) The lateral movement of the probe over the PDMS surface during the friction experiment involves breaking of the contact to the soft substrate, which is expected to occur in a peeling-like fashion. Reported peeling experiments on structured PDMS surfaces have demonstrated that crack propagation can be hindered by microstructures due to arrest of the crack at edges.[37,38] This leads to higher peeling forces on structured substrates.

When the aspect ratio of the pillars increased, the friction force decreased and almost no friction was observed on patterns with pillars with aspect ratio 2, both in wet and dry states. A microscopic image of the contact surface during the experiment showed that the pillars with large aspect ratios bent and stuck together during the lateral displacement, thereby losing the contact to the surface (Figure 6c). As a consequence, only low static and dynamic frictional forces occurred. These results show that the benefit of structured surfaces for friction critically depends on the geometry of the surface design. Only structures with aspect ratio 0.35 provided sufficient lateral stability against bending and were advantageous for friction purposes. Pillars with higher aspect ratios easily bent and collapsed during shear, resulting in a low friction performance in dry and wet conditions.

Hydrophobic flat surfaces displayed higher friction than the microstructured ones with flat terminals (Supporting Information, Figure SI-14). The same friction values were obtained in the presence or absence of fluid, indicating that the non-wetting water was immediately displaced from the contact area independently of the surface structure. Microstructured surfaces with pillars with aspect ratio 0.7 also showed very low friction as a consequence of collapse during shear. In summary, no particular benefit of surface structure for friction was visible in the hydrophobic, non-wetting case.

3.5. Wetting Properties of Tree-Frogs' Toe-Pads and Secretion

In order to identify which of the described cases represents the frog's attachment mechanism, the contact angle of the fluid secretion on hydrophilic and hydrophobic surfaces and the contact angle of tree-frog toe-pads were measured. The toe-pad secretion from the tree-frog *Litoria caerulea* was gained by allowing the frog to walk up on a clean glass surface and collecting the released fluid from toe-pad footprints using a capillary tube. Microdroplets (2 μL) of the frog's secretion had static contact angles lower than 10° on both hydrophilic (silica) and hydrophobic surfaces (Teflon), indicating that they are able to wet both types of surfaces. The contact angle of the frog toe-pad was measured by putting a drop of water onto a frog toe-pad. The water droplet immediately spread over the pad surface, indicating that the frog's adhesive surface is hydrophilic. In summary, the tree-frog's wet adhesive case corresponds to a hydrophilic surface in the presence of a wetting liquid.

4. Conclusions

The adhesion of tree-frog like microstructured surfaces in the presence of a liquid involves capillary interactions and direct contact forces. The magnitude of the contribution of these two forces to the net adhesion force depends on how the liquid wets the surface. Viscous and suction forces do not pay any significant contribution.

- In a wetting case, capillary interactions dominate. The resulting adhesion force is independent of the presence of the microstructure or its geometrical design and it decreases with increasing fluid volume.
- With a non-wetting liquid, the surface microstructure can be highly beneficial for adhesion. Depending on the surface design, the magnitude of the direct contact force can surpass that of capillary interactions. In this case, the rules for gecko-like dry adhesives also apply to tree-frog-like wet adhesives. In particular, T-shaped microstructures, being the most favourable ones for dry adhesion, are also highly beneficial for wet adhesion.

A different effect of the microstructure was observed for friction purposes.

- A microstructured surface can show significantly higher friction than a flat one in the presence of a wetting liquid. The shear forces effectively drain the wetting liquid out of the contact area only if surface structures are present. Under these conditions, microstructured surfaces containing low-aspect-ratio features that do not bend or collapse during shear can establish direct contact and greatly surpass the friction performance of the flat surface.
- In the presence of a non-wetting liquid, the shear forces drain the liquid from flat and microstructured surfaces. Our flat terminated microstructured surfaces had lower friction than flat ones. However, this situation can be different with T-shaped pillar designs which have been demonstrated to be beneficial for dry friction.[39]

In view of these results and taking into account that tree-frog attachment pads are hydrophilic, it seems that the surface structure in tree-frog toe-pads has been developed for climbing on wet surfaces, when shear (friction) forces are involved. Interestingly, the epithelial cells of the frogs have a diameter of 10–15 μm and are separated at their distal ends by 5–7 μm channels. This gives an aspect ratio of ca. 0.5 and, therefore, enough mechanical stability to withstand shear forces without collapsing. On the other hand, our results demonstrate that the same surface design can also significantly help for adhesion purposes in the presence of a non-wetting liquid.

Supporting Information

Supporting Information is available from the Wiley Online Library or from the author.

Acknowledgements

The authors thank the Deutsche Forschungs Gemeinschaft for financial support within the program SPP1420 "Biomimetic Materials Research: Functionality by Hierarchical Structuring of Materials" (Projects CA880/1, BU 1556/26) and Thomas Endlein (University of Glasgow) for help with the friction measurements.

Received: July 18, 2012
Published online: October 9, 2012

[1] K. Autumn, in *Biological Adhesives*, (Eds: A. M. Smith, J. A. Callow), Springer, Berlin **2006**, 225.
[2] E. Arzt, S. Gorb, R. Spolenak, *Proc. Nat. Acad. Sci. USA* **2003**, *100*, 10603.
[3] B. X. Zhao, N. Pesika, H. B. Zeng, Z. S. Wei, Y. F. Chen, K. Autumn, K. Turner, J. Israelachvili, *J. Phys. Chem. B* **2009**, *113*, 3615.
[4] L. F. Boesel, C. Greiner, E. Arzt, A. del Campo, *Adv. Mater.* **2010**, *22*, 2125.
[5] J. Cui, D.-M. Drotlef, I. Larraza, J. P. Fernández-Blázquez, L. P. Boesel, C. Ohm, M. Metzger, R. Zentel, A. del Campo, *Adv. Mater.* **2012**, *26*, 4601.
[6] S. Reddy, E. Arzt, A. del Campo, *Adv. Mater.* **2007**, *19*, 3833.
[7] W. J. P. Barnes, *MRS Bull.* **2007**, *32*, 479.
[8] W. J. P. Barnes, C. Oines, J. M. Smith, *J. Comp. Physiol. A* **2006**, *192*, 1179.
[9] W. Federle, W. J. P. Barnes, W. Baumgartner, P. Drechsler, J. M. Smith, *J. R. Soc. Interface* **2006**, *3*, 689.
[10] G. Hanna, W. J. P. Barnes, *J. Exp. Biol.* **1991**, *155*, 103.
[11] I. Scholz, W. J. P. Barnes, J. M. Smith, W. Baumgartner, *J. Exp. Biol.* **2009**, *212*, 155.
[12] J. M. Smith, W. J. P. Barnes, J. R. Downie, G. D. Ruxton, *J. Comp. Physiol. A* **2006**, *192*, 1193.
[13] W. J. P. Barnes, P. J. P. Goodwyn, M. Nokhbatolfoghahai, S. N. Gorb, *J. Comp. Physiol. A* **2011**, *197*, 969.
[14] B. N. J. Persson, *J. Phys.-Condens. Matter* **2007**, 19.
[15] H. J. Butt, W. J. P. Barnes, A. del Campo, M. Kappl, F. Schonfeld, *Soft Matter* **2010**, *6*, 5930.
[16] S. B. Emerson, D. Diehl, *Biol. J. Linnean Soc.* **1980**, *13*, 199.
[17] M. Kober, E. Sahagun, P. Garcia-Mochales, F. Briones, M. Luna, J. J. Saenz, *Small* **2010**, *6*, 2725.

[18] X. J. Zhang, Y. Liu, Y. H. Liu, S. I. U. Ahmed, *Chinese Sci. Bull.* **2009**, *54*, 1648.
[19] X. J. Zhang, X. Yi, S. I. U. Ahmed, M. Kosinskiy, Y. H. Liu, J. A. Schaefer, *Tribol. T* **2010**, *53*, 280.
[20] E. Cheung, M. Sitti, *J. Adhes. Sci. Technol.* **2008**, *22*, 569.
[21] M. Varenberg, S. Gorb, *J. R. Soc. Interface* **2008**, *5*, 383.
[22] M. Varenberg, S. N. Gorb, *Adv. Mater.* **2009**, *21*, 483.
[23] A. del Campo, C. Greiner, E. Arzt, *Langmuir* **2007**, *23*, 10235.
[24] C. Greiner, A. del Campo, E. Arzt, *Langmuir* **2007**, *23*, 3495.
[25] A. del Campo, C. Greiner, *J. Micromech. Microeng.* **2007**, *17*, R81.
[26] A. del Campo, C. Greiner, I. Alvarez, E. Arzt, *Adv. Mater.* **2007**, *19*, 1973.
[27] A. del Campo, I. Alvarez, S. Filipe, M. Wilhelm, *Adv. Funct. Mater.* **2007**, *17*, 3590.
[28] P. Drechsler, W. Federle, *J. Comp. Physiol. A* **2006**, *192*, 1213.
[29] H.-J. Butt, M. Kappl, *Surface and Interfacial Forces*, Wiley-VCH, Weinheim, Germany **2010**.
[30] H. J. Butt, M. Kappl, *Adv. Colloid Interface Sci.* **2009**, *146*, 48.
[31] K. L. Johnson, K. Kendall, A. D. Roberts, *Proc. R. Soc. Lon. Ser.-A* **1971**, *324*, 301.
[32] E. J. De Souza, M. Brinkmann, C. Mohrdieck, E. Arzt, *Langmuir* **2008**, *24*, 8813.
[33] E. Barthel, C. Fretigny, *J. Phys. D Appl. Phys.* **2009**, 42.
[34] J. A. Greenwood, K. L. Johnson, *Philos. Mag. A* **1981**, *43*, 697.
[35] M. Deruelle, L. Leger, M. Tirrell, *Macromolecules* **1995**, *28*, 7419.
[36] L. Leger, C. Creton, *Philos. T. R. Soc. A* **2008**, *366*, 1425.
[37] A. Ghatak, *Phys. Rev. E* **2010**, 81.
[38] C. Poulard, F. Restagno, R. Weil, L. Leger, *Soft Matter* **2011**, *7*, 2543.
[39] M. Varenberg, S. Gorb, *J. R. Soc. Interface* **2007**, *4*, 721.